Numerical simulation of turbulent flows in a channel with a series of groynes by ZDES

***†J.X. Zhang[1,2]**

[1]MOE Key Laboratory of Hydrodynamics, Shanghai Jiao Tong University, China
[2]School of Naval Architecture, Ocean and Civil Engineering, Shanghai Jiao Tong University, China

*Presenting author: zhangjingxin@sjtu.edu.cn
†Corresponding author: zhangjingxin@sjtu.edu.cn

Abstract

In the present work, the hydrodynamics in a straight open channel constructing a multiple-embayment groyne field on one of its sides is investigated by numerical simulations. The open channel is composed of a flat bottom in the main channel and a gradual slope toward one of the sides with a ratio 1:3. A series of five embayment are constructed on the slope, and the ratio of the embayment's length to width is specified as 3. A thorough analysis of the three-dimensional flow characteristics was carried out by Zonal detached-eddy simulation (ZDES) model. The numerical simulation highlights the turbulent coherent structures induced by groynes, including local horseshoe vortex (HV) around the groyne tip, shedding vortex (SV) from the groyne and the mixing layer flow at the channel-embayment interface. Both the instantaneous and the mean flows show a spatial evolution of turbulence in the main channel and embayment, which reveals different coherent structures from the upstream embayment to the downstream embayment. The analysis of the large-scale eddies, which populates the mixing between the channel and embayment, are contributed to investigate the mechanisms of fluid mixing, mass transportation and exchange, and some issues about hydraulic engineering.

Keywords: Hydrodynamics, channel flow, groynes, Zonal-DES, free surface flow

Introduction

Groynes are commonly built with an angle to the main flow to fulfill multiple objectives. One of the most usual targets is to maintain the channel navigability by keeping the flow away from the banks and increasing the velocity in the channel as well as increasing the energy of sediment transportation. There are also other objectives, for example, restoring fish habitat by degrading the river current [1]. Because the embayment region between successive groynes acts as a dead water zone, the fluid and dissolved mass exchange ratio decreases and the residence times of matter are much larger, which raises an eco-hydraulic problem [2].

The turbulence coherent structures are dominated by the channel geometry and groyne shapes, including the groyne orientation, space of the embayment, emerged, submerged, permeable and the groyne tip shape [3]-[4]. On the other hand, the large-scale eddies populate the fluid mixing between the main channel and embayment. Most of the knowledge about the dynamics of turbulent flows in groyne flows comes from experimental scale-model researches by means of experimental techniques to capture the mean velocity and instantaneous turbulence quantities [5]-[6].

Besides of experimental researches, the numerical model is much more efficient to capture some quantitative hydrodynamic factors of the groyne field flows. The early numerical simulation works were based on the RANS models [7]-[8], which was contributed to the mean recirculation simulations. Large eddy simulation (LES) method is prior to the RANS model in predicting large-scale eddies, which is considered as the key dynamic force dominating the mass transportation and exchange in the groyne area [9]-[11]. Much more hydrodynamic mechanisms have been highlighted by LES, but the high computational cost hinders the practical applications in large-scale channel flows, for example the natural river flows. A family of hybrid RANS/LES model, named as detached-eddy simulation (DES) is practical to promote the high-resolution numerical simulations in practical hydraulic engineering simulation.

In the present paper, a Zonal detached-eddy simulation (ZDES) model is developed to simulate free surface flows [12], and then is employed to study the turbulent flows in a channel composed of a flat bottom in the main channel and a slope bottom along one side with a series of emergent groynes constructed on the slop bottom with a constant ratio of the embayment length to width. It is feasible using ZDES to investigate the 3D flow features referring to turbulent fluctuations, distributions of turbulent energy, and the bed shear stress distribution.

Numerical method and simulation setup

Governing Equations

In the present 3D numerical model, the total pressure is split into the hydrostatic component $p_h = \rho g\left(\zeta - z\right)$ and non-hydrostatic component p_n. The 3D governing equations are written in a conversation form:

$$\frac{\partial \zeta}{\partial t}+\frac{\partial q_x}{\partial x}+\frac{\partial q_y}{\partial y}+\frac{\partial q_\sigma}{\partial \sigma}=0 \tag{1}$$

$$\frac{\partial q_x}{\partial t}+\frac{\partial q_x u}{\partial x}+\frac{\partial q_x v}{\partial y}+\frac{\partial q_x \tilde{\omega}}{\partial \sigma}=-gD\frac{\partial \zeta}{\partial x}-\frac{D}{\rho_0}\frac{\partial p_n}{\partial x}+\frac{\partial}{\partial x}\left(\upsilon_t\frac{\partial q_x}{\partial x}\right)+\frac{\partial}{\partial y}\left(\upsilon_t\frac{\partial q_x}{\partial y}\right)+\frac{1}{D}\frac{\partial}{\partial \sigma}\left(\frac{\upsilon_t}{D}\frac{\partial q_x}{\partial \sigma}\right) \tag{2}$$

$$\frac{\partial q_y}{\partial t}+\frac{\partial q_y u}{\partial x}+\frac{\partial q_y v}{\partial y}+\frac{\partial q_y \tilde{\omega}}{\partial \sigma}=-gD\frac{\partial \zeta}{\partial y}-\frac{D}{\rho_0}\frac{\partial p_n}{\partial y}+\frac{\partial}{\partial x}\left(\upsilon_t\frac{\partial q_y}{\partial x}\right)+\frac{\partial}{\partial y}\left(\upsilon_t\frac{\partial q_y}{\partial y}\right)+\frac{1}{D}\frac{\partial}{\partial \sigma}\left(\frac{\upsilon_t}{D}\frac{\partial q_y}{\partial \sigma}\right) \tag{3}$$

$$\frac{\partial q_z}{\partial t}+\frac{\partial q_z u}{\partial x}+\frac{\partial q_z v}{\partial y}+\frac{\partial q_z \tilde{\omega}}{\partial \sigma}=-\frac{1}{\rho_0}\frac{\partial p_n}{\partial \sigma}+\frac{\partial}{\partial x}\left(\upsilon_t\frac{\partial q_z}{\partial x}\right)+\frac{\partial}{\partial y}\left(\upsilon_t\frac{\partial q_z}{\partial y}\right)+\frac{1}{D}\frac{\partial}{\partial \sigma}\left(\frac{\upsilon_t}{D}\frac{\partial q_z}{\partial \sigma}\right) \tag{4}$$

where g is gravitational acceleration, ζ is the free surface elevation. When the non-hydrostatic component p_n is ignored, the vertical momentum equation is also neglected, and the system degenerates to the common shallow water equations with only two horizontal momentum equations and one continuity equation, which is also named as hydrostatic model. In order to fit the free surface and the uneven bottom boundary, the vertical coordinate z is transformed to the σ coordinate. In the governing equations. The new variables $q_x = Du, q_y = Dv, q_z = Dw, q_\sigma = D\tilde{\omega}$ are introduced instead of the velocity u,v and w, and the vertical velocity in σ coordinate is calculated by the following formula:

$$q_\sigma=\frac{q_z}{D}-\frac{q_x}{D}\left(\sigma\frac{\partial D}{\partial x}+\frac{\partial \zeta}{\partial x}\right)-\frac{q_y}{D}\left(\sigma\frac{\partial D}{\partial y}+\frac{\partial \zeta}{\partial y}\right)-\left(\sigma\frac{\partial D}{\partial t}+\frac{\partial \zeta}{\partial t}\right) \tag{5}$$

Turbulence model

The eddy viscosity coefficient υ_t is determined based on the one-equation S-A model. The working variable $\tilde{\upsilon}$ obeys the following transport equation

$$\frac{D\tilde{\upsilon}}{Dt}=c_{b1}\tilde{S}\tilde{\upsilon}-c_{w1}f_w\left[\frac{\tilde{\upsilon}}{d}\right]^2+\frac{1}{\tilde{\sigma}}\left\{\nabla\cdot\left[\left(\upsilon+\tilde{\upsilon}\right)\nabla\tilde{\upsilon}\right]+c_{b2}\left(\nabla\tilde{\upsilon}\right)^2\right\} \tag{6}$$

The eddy viscosity υ_t is given by

$$\upsilon_t=\tilde{\upsilon}f_{v1} \tag{7}$$

where $f_{v1}=\frac{\chi^3}{\chi^3+c_{v1}^3}$, $\chi\equiv\frac{\tilde{\upsilon}}{\upsilon}$. υ is the molecular viscosity. Here $\left|\bar{S}\right|$ is the magnitude of the strain rate tensor, $\tilde{S}=\left|\bar{S}\right|+\frac{\tilde{\upsilon}}{\kappa^2d^2}f_{v2}$, $f_{v2}=1-\frac{\chi}{1+\chi f_{v1}}$.The function f_w is calculated as $f_w=g\left[\frac{1+c_{w3}^6}{g^6+c_{w3}^6}\right]^{1/6}$, $g=r+c_{w2}\left(r^6-r\right)$, $r\equiv\frac{\tilde{\upsilon}}{\tilde{S}\kappa^2d^2}$. The constants in the above equations are $c_{b1}=0.1355$, $\tilde{\sigma}=2/3$, $c_{b2}=0.622$, $\kappa=0.41$, $c_{w1}=c_{b1}/\kappa^2+\left(1+c_{b2}\right)/\tilde{\sigma}$, $c_{w2}=0.3$, $c_{w3}=2.0$, $c_{v1}=7.1$.

The DES model concerns the destruction term in the transport Equation (6), and the distance d to the solid wall is replaced by a modified length $\tilde{d}$. In the present model, the unstructured grid is used in the horizontal plane and a structured sigma-grid is used in the vertical direction, and the $\tilde{d}$ is calculated by

$$\tilde{d}=\min\left(d,C_{DES}\Delta\right)\text{, with }\Delta=\max\left(\sqrt{4A/\pi},\Delta z\right) \tag{8}$$

where A is the horizontal mesh area; C_{DES} is 0.65. There is a layer near the solid wall where $\tilde{d}=d$, which is referred to as the traditional "RANS" zone, and the simulation is turned into "LES" zone above this layer where $\tilde{d}=C_{DES}\Delta$.

The model-stress depletion (MSD) is one severe problem of the RANS/LES hybrid model, which is pronounced for the DES when the switch from RANS to LES takes place in the boundary layer, so Spalart [13] proposed a new version of DES, i.e. DDES, to delay the switch from RANS to LES. Shur et al. [14] developed a new model, named IDDES, for the simulation with an ambiguous grid scale, which can solve the MSD problem by modifying the turbulent length scale, initial condition and inflow condition. Keating et al. [15] presented a dynamic stochastic forcing method, which significantly speeds up the transition resulting in more accurate predictions of the velocity fluctuation. The Zonal-DES approach is well adopted to handle separated flows in which strong instabilities develop rapidly, thus overwhelming the turbulence inherited from upstream boundary layers [16]-[17]. In the present model, a Zonal-DES model is developed by means of modifying the functions f_{v1}, f_{v2} and f_w as shown in (9) and adopting a new sub-grid length scale $\Delta=\left(A\Delta z\right)^{1/3}$ in the LES computational domain.

$$f_{v1}=0,\ f_{v2}=0,\ f_w=1 \tag{9}$$

Numerical scheme

A predictor-corrector scheme is used in the numerical method [18]. In summary, the flow driven by hydrostatic pressure is calculated as the predictor step, and then the flow driven by non-hydrostatic pressure is further resolved in the corrector step. The grid system is composed of unstructured horizontal grids and multi-layers in the vertical direction. The governing equations are discretized based on finite volume method (FVM). The 2nd-order total variation diminishing (TVD) scheme, sometimes referred to as the modified-flux approach. In the present numerical model, the OSHER scheme is adopted. In the corrector step, the Poisson-type equation for the non-hydrostatic pressure is numerically obtained by the pre-conditioned BI-CGSTAB approach. The in-house codes are paralleled by OpenMP library.

Simulation setup

The sketch of the computational domain is shown in Fig.1, which is composed of a flat main channel bottom and a slope bottom along one side. The slope bottom extends from the bank into the main channel with a constant slope 1 in 3, which is also revealed in Fig.2. The groynes are emerged and perpendicular to the main flow direction. The depth in the main channel $D = 0.2m$ was chosen as the length scale. The mean velocity $U = 0.22m/s$ in the main channel was chosen as the velocity scale. The Reynolds number was $\mathrm{Re} = UD/\upsilon = 44,000$, and Froude number $Fr = U/\sqrt{gD} = 0.2$. In the computational domain, x = stream wise direction, z = vertical direction (originating on the still water level), and in the transversal direction, $y = 0$ corresponds to the sidewall. The domain extends upstream 20D of the first embayment and 50D downstream of the last embayment. The thickness of the groynes is 0.25D. The width (3D) over length (9D) ratio of each embayment is 1/3. The depth in the embayment area increases from 0.15D at the sidewall to D with a slope of 1:3, and the horizontal length of the slope in the embayment is 2.5D, which is shorter than the groyne length 3D (Fig.2). The length scale of the embayment guarantees the applicability of the SWE (shallow water equation) in hydrostatic mode, but the groyne tip and the presence of the change of depth between the main channel and the embayment are likely to induce strong 3D effects. Consequently, the present non-hydrostatic model is needed for the flow simulations.

In ZDES by means of S-A model as it stands in the above section, the grid scale is strictly limited in the wall units: $\Delta_\perp^+ = O(1)$ at the wall. We maintained $\Delta_\perp^+ \approx 1$ between the first grid point to the nearest wall, and stretched the grid size with a ratio of 1.15 away the solid wall until the grid size meets the criterion for LES simulations. For open channel flows, Hinterberger et al.[10] proposed a valuable reference grid size in LES. Because the large-scale eddies in open channel flow are limited by the characteristic length, i.e. the water depth h, the grid size was properly designed in the range of $(\frac{1}{20} \sim \frac{1}{10})h$. The total number of the meshes is about 9 million.

The free surface boundary can be captured by the stretching σ grid, which is high efficient in the simulation of free surface motion. The sidewall and the bottom were considered as non-slip boundaries, and the lateral wall opposite the groynes was considered as slip boundary. The grid scale was designed to ensure the local LES domain only covering the embayment, and beyond the LES area, the RANS domain extending to the inlet and outlet boundaries. A steady inflow boundary condition was used, and the flow in the inlet section was fully turbulent obtained by means of a precalculated fully-developed open channel flow simulation. In the outlet section, a fixed water level was specified and a convective flux condition was used in the discretizing the momentum equations.

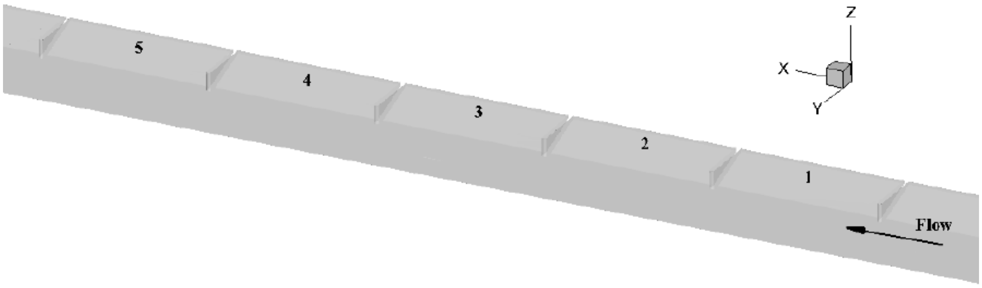

Fig. 1 Sketch showing computational domain with five shallow embayment.

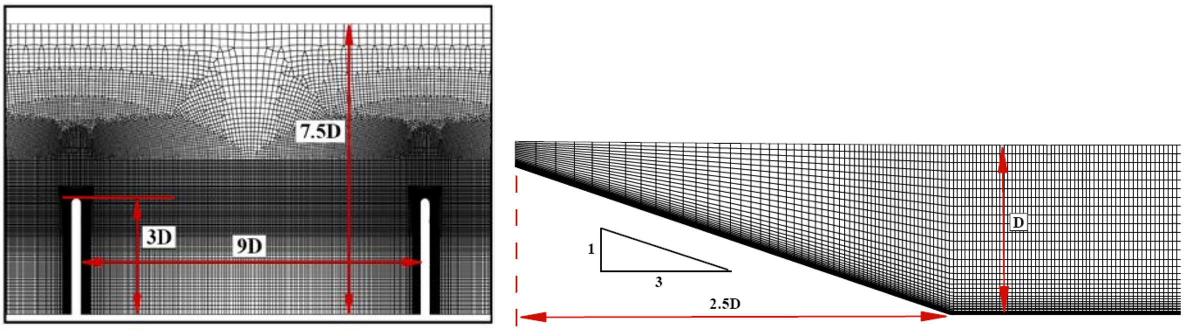

(a) (b)

Fig.2 Computational mesh: (a) mesh in a horizontal plane; (b) mesh in a vertical cross section

Results and Discussion

The simulation was firstly run until the transients were eliminated, i.e. being fully turbulent. Statistics were further calculated using the instantaneous flow fields over the next $120D/U$. The present work was focused on the evolution of the turbulent flows from the first groyne to downstream. And the instantaneous and mean flow were analyzed to investigate the hydrodynamics.

Instantaneous flow

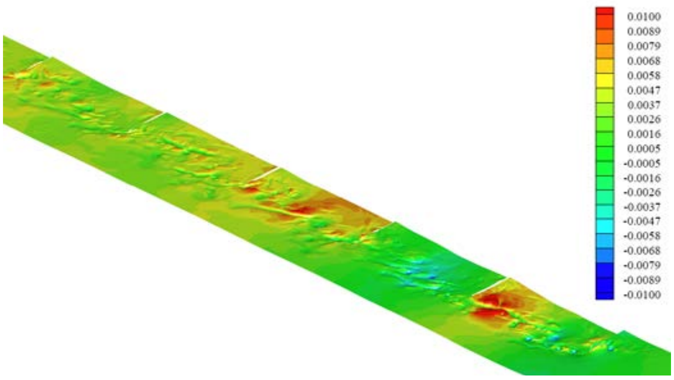

Fig.3 The instantaneous free surface

The instantaneous free surface reveals the evolution of the turbulent flows induced by the groynes on the uneven bottom. Fig.3 shows a snapshot of the free surface. The vortical structures beneath the free surface deform the geometry of free surface. Surface patterns, such as upwelling, downdraft, and ripples were predicted in the present simulations. A series of regular surface downdraft are observed justly downstream of the first groyne, and these downdraft surface motion are gradually weakened in the following embayment. This surface pattern corresponds to the shedding vortex originated from the tip of the groynes. At the channel-embayment interface, a large-scale ripple structure is observed, which dominates the fluid exchange between the main channel and the embayment. The present simulations show no identical free surface pattern until the last groyne.

It is expected that small-scale vortical structures are predicted by the ZDES model. A positive isovalue of criterion Q was used to show the turbulent structures, which defines as the vortex tubes in the regions where the second invariant of the velocity gradient tensor is positive. Fig.4 shows the instantaneous Q (= 6) in the groyne area, in which the small-scale vortical structures develop very quickly originated from the first groyne. In order to investigate the details of the coherent structures, the local vortical structures identified by isovalue of Q in embayment 1 and embayment 3 are presented in Fig.5. At instantaneous $t = t_0$, there are mainly three distinct vortical structures around the fire groyne. The necklace-like vortices (NV) originate from the upstream groyne face near the free surface. The organized shedding vortex (SV) is observed beneath the free surface, and the horseshoe vortex (HV) is formed at the basement of the groyne. The SV gradually decays downstream of the first groyne. The near surface vortical streak becomes oriented relatively parallel to the free surface, which corresponds to the mixing layer induced by the upstream groyne. At instantaneous $t = t_0 + 3D/U$, the NV degenerates, but the HV and the SV become intensity and develop gradually downstream. At instantaneous $t = t_0 + 5D/U$, the SV continually develop downstream along with merging and decaying with ambient vortices . The large-scale HV breaks down during the interaction with small-scale vortices. In embayment 3 area, the similar vortical structures are observed in the snapshot of the flow field shown in Fig.5, but the SV and HV at the basement are not obviously formed, which is likely because of the attenuation of the incident flows. However, a large-scale vortical structure penetrating into the embayment is observed. The instantaneous coherent structures of the turbulent flow are corresponded to the flow separating at the tip of the groynes and the mixing layer flow formed by the high speed channel flows and the low speed embayment flows at the interface. Conversely, the large-scale vortices predominate the mass exchange between the main channel and the embayment, the local scouring and the suspended sediment transportation.

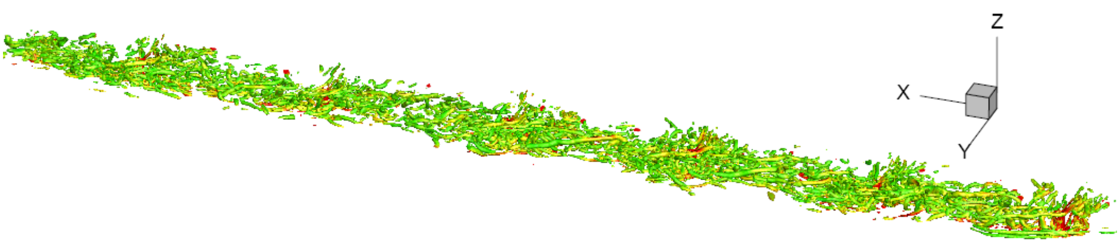

Fig.4 The coherent structures of turbulent flows identified by Q flooded by vorticity.

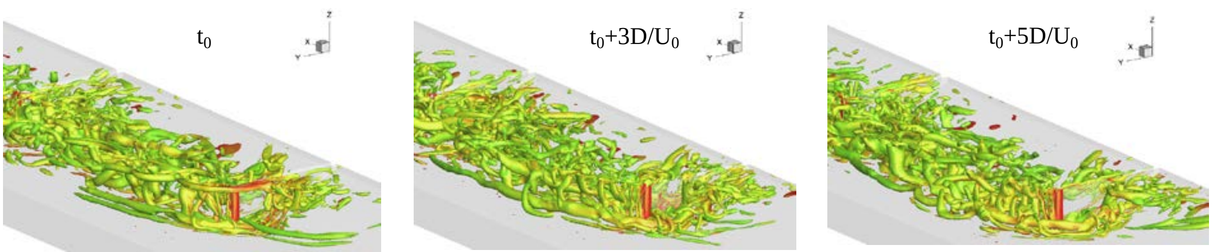

(a) Embayment 1

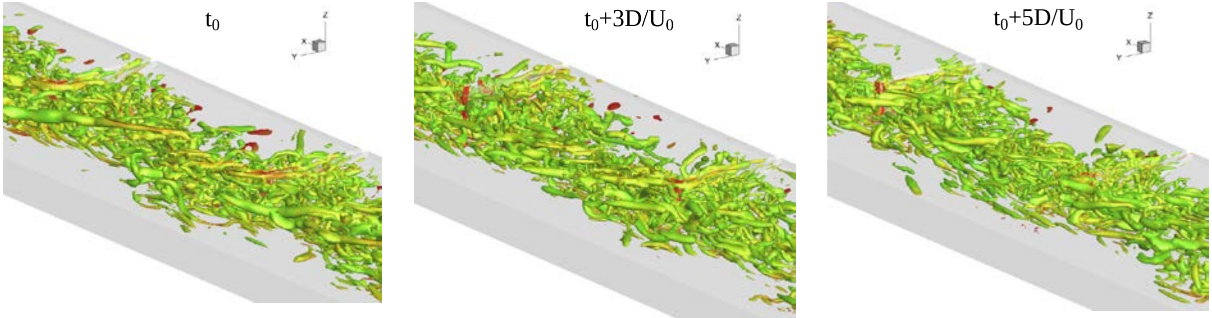

(b) Embayment 3

Fig. 5 The coherent structures of the turbulent flow identified by Q: (a) Embayment 1, and (b) Embayment 3.

Time-averaged mean flow

The mean flows were calculated using the instantaneous flow fields over $120D/U$. The random small-scale vortices are disappear in the mean velocity field, and the related steady flow patterns contribute to analyze the long-term hydrodynamics in the channel flows with groynes.

Fig.6 shows the rough mean velocity streamlines in the computational domain. A one-gyre circulation is observed located in the corner in front of the first groyne, and the local streak is highly three dimensional. A two-gyre circulation pattern is distinctly observed in embayment 1, embayment 3, and embayment 5, but the similar recirculation is not clearly observed in the other embayment. Fig.6 reveals that the identical flow pattern in the embayment has not fully developed.

The mean velocity streamlines present the long-term fluid particle's kinematic path, and can be qualitatively used to analyze the mean mass exchange between different reaches. Fig.7 (a) clearly shows a two-gyre recirculation in embayment 3. Affected by the change bottom topography, the mean recirculation reveals a distinct 3D pattern rather than a 2D pattern commonly observed in shallow water channel flows. One single streamline originated from the upstream is elaborately selected to show the path of one fluid particle motion (Fig.7 (b)), which roughly presents one possible mass transport route. The scale of the secondary gyre at the corner is commonly smaller than that observed in groyne flow with the similar ratio of length to width but on flat bottom.

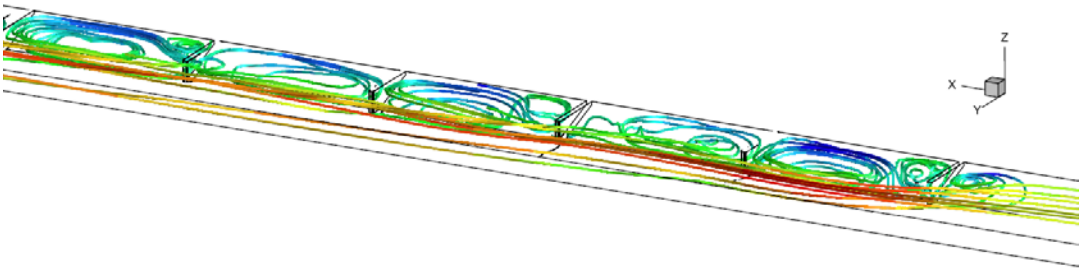

Fig. 6 Mean velocity streamlines flooded by stream wise velocity.

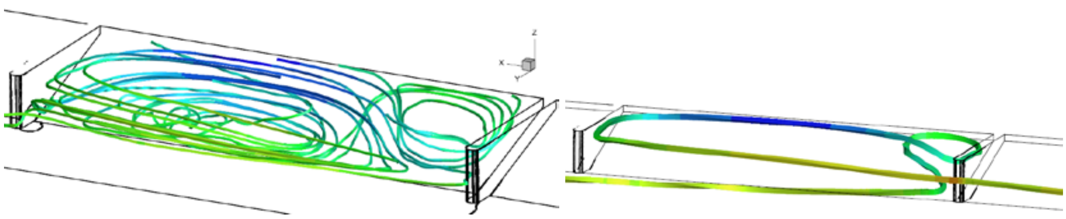

a) mean velocity streamlines b) one selected velocity streamline

Fig.7 Local mean velocity streamlines showing the recirculation in embayment 3.

Fig.8 reveals the mean velocity streamlines in the horizontal plane at different vertical position, i.e. near the surface ($\sigma = -0.05$), at the mid-depth ($\sigma = -0.5$), and near the bottom ($\sigma = -0.95$). $\sigma \in [-1,0]$ presents the relative depth. The panels from top to bottom in Fig.8 correspond to the embayment in the stream wise. The mean velocity streamlines at the mid-depth in front of the first groyne reveal a large-scale clockwise recirculation and a small-scale unclockwise recirculation upstream of it. The recirculation pattern near the free surface is a bit different, especially in the area very near to the tip of the groyne. The surface ripples likely effect the local flows shown in Fig.8. Near the bottom, some complex structures presented by saddle points, nodes and spiral or focus points are observed. The details of the characteristic streamlines or singular points clearly describe the flow structures, for example, the separation of the boundary flows. In the present simulation, an identical flow pattern have not developed until the last groyne, which can be observed from the streamlines not only in the near surface plane, but also the mid-depth plane or the adjacent bottom plane. Justly analyzing the recirculation in the mid-depth plane shown in the middle column panels in Fig.8, the size of a two-gyre is different among the five embayment. The relative size of the secondary gyre to the main one is about identical in embayment 4 and 5, which is roughly considered as an identical flow pattern. The two-gyre flow pattern is affected by the incident flow condition and the geometry of the computational domain. A periodic open boundary condition is commonly used in numerical simulations of flow passing one embayment, in which the computational cost decreases because of the smaller computational domain. The simulation of the flow passing series of groynes give rise to the selection of the periodic boundary position.

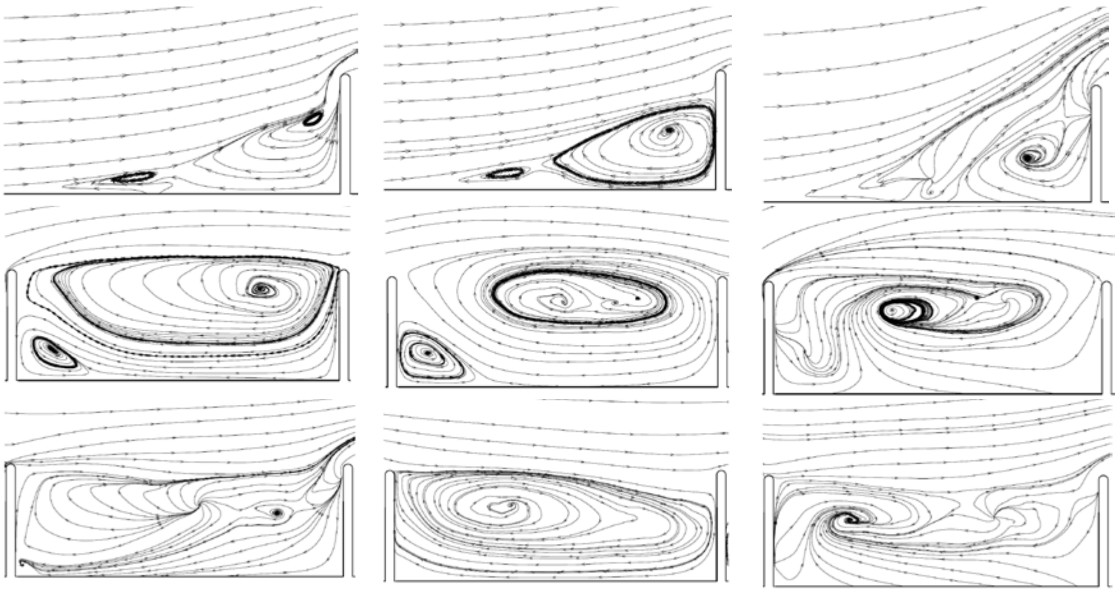

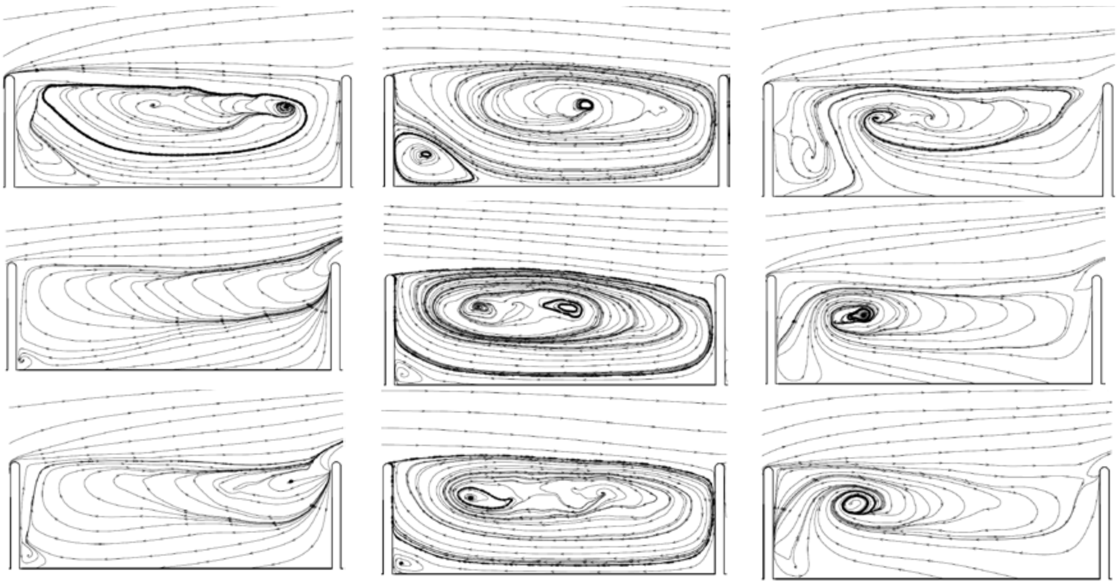

a) near the free surface b) at mid-depth c) near the bottom

Fig. 8. Mean velocity streamlines in horizontal planes along the groynes.

Fig.9 shows the distribution of the mean turbulent kinetic energy (TKE) in the horizontal planes from the surface to the bottom. The maximum value occurs near the tip of the first groyne near the free surface and near the basement, which reveals relative stronger flow fluctuations compared to the flow in the mid-depth. The higher level of TKE in embayment 1 corresponds the stronger incident flow and the sharp distortion of the local streamlines around the frontal groyne tip, and the next groynes are sheltered in the downstream flows. Because of the weakened incident flow and the little distortion of the local streamlines around the groyne tip, the level of TKE decreases downstream.

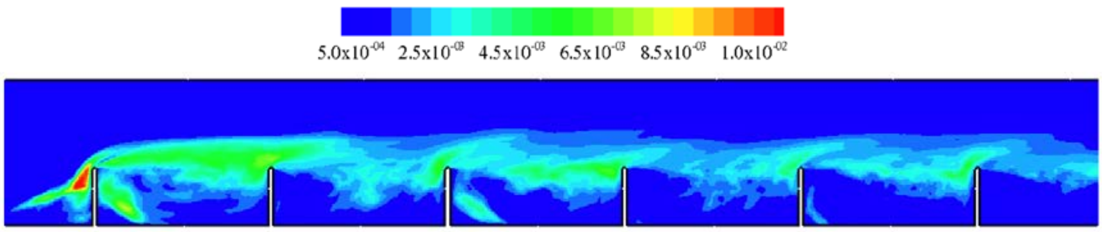

a) near the free surface

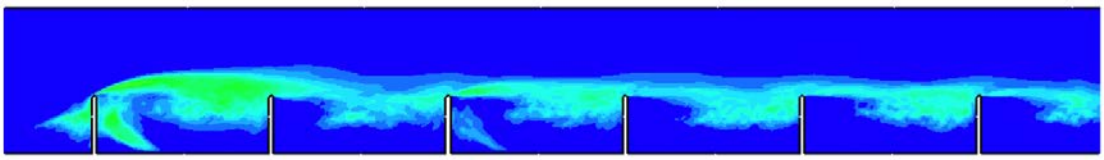

b) at mid-depth

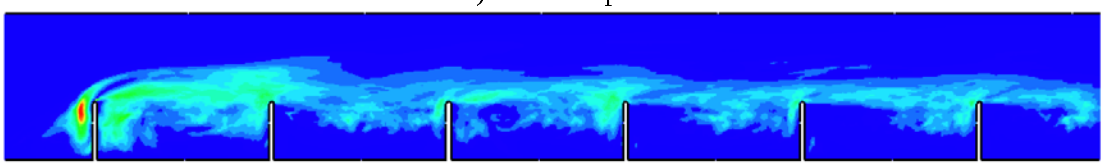

c) near the bottom

Fig. 9 The mean turbulent kinetic energy in horizontal planes.

Conclusions

A 3D non-hydrostatic numerical model was developed and used to investigate the channel flow with a series of groynes constructed on a slope along one side. The ZDES was used to simulate the turbulence by aid of its superiority in predicting small-scale vortical structures compared to RANS model. The simulations deeply investigate the turbulent coherent structures induced by the groynes and the composited topography. The attention were focused on the spatial evolution of the vortices not only in the streamwise, but also in the vertical direction. The analysis of the coherent structures is benefit to investigate the mechanism of the hydrodynamic forces and the mass advection or exchange across the chaneel-embayment interface.

Acknowledgements

This work was jointly sponsored by the National Natural Science Foundation of China (No. 11572196) and the National Basic Research Program of China (973 Program, No. 2014CB046200).

References

[1] Shields, F.D., Cooper, C.M., and Knight, S.S. (1995). Experiments in stream restoration. J. Hydrauli.Eng., 121, 494-502.

[2] Engelhardt, C., Kruger, A., Sukhodolov,A., and Nicklisch, A. (2004). A study of phytoplankton spatial distributions, flow structure and characteristics of mixing in a river reach with groynes. J. Plankton Res., 26, 1351-1366.

[3] Sukhodolov A., Uijttewaal W.S.J., and Engelhardt C. On the correspondence between morphological and hydrodynamical patterns of groyne fields. Earth Surface Processes and Landforms, 2002, 27: 289-305.

[4] Weitbrecht V., Scocolofsky S.A., and Jirka G.H. Experiments on mass exchange between groin fields and main stream in rivers. Journal of Hydraulic Engineering, 2008, Vol. 134, No. 2, pp. 173-183.

[5] Uijttewaal W.S.J., Lehmann D., and van Mazijk A. Exchange processes between a river and its groyne fields: model experiments. Journal of Hydraulic Engineering, 2001, Vol.127, No.11, pp. 928-936.

[6] Uijttewaal W.S.J. Effects of groyne layout on the flow in groyne fields: laboratory experiments. Journal of Hydraulic Engineering, 2005, Vol.131, No.9, pp.782-791.

[7] Peng, J., Kawahara, Y., and Huang, G. (1999a). Evaluation of modified k-ε models in simulating 3D flows over submerged spur dikes. Proc., Turbulence and Shear Flow-1, First Int. Symp., S. Banerjee and J.K. Eaton,eds., Santa Barbara, Calif.

[8] Peng, J., Tamai, N., Kawahara, Y., and Huang, G. (1999b). Numerical modeling of local scour around spur dikes. Proc., 28th IAHR Congress, Graz, Austria.

[9] Uijttewall, W., and van Schijndel, S.A.H. (2004). The complex flow in groyne fields: Numerical modeling compared with experiments. Proc. River Flow 2004, Naples, Italy, 1331-3838.

[10] Hinterberger, C. (2004). Three-dimensional and depth-average large eddy simulation of shallow water flows. Ph.D. thesis, karlsruhe Univ., Karlsruhe, Germany.

[11] McCoy, A., Constantinescu G., and Weber L.J. Numerical investigation of flow hydrodynamics in a channel with a series of groynes. Journal of Hydraulic Engineering, 2008, Vol. 134, No.2, pp. 157-172.

[12] Zhang, J.X., Wang X.K., Liang D.F., and Liu H. (2015). Application of detached-eddy simulation to free surface flow over dunes. Engineering Applications of Computational Fluid Mechanics, 2015, Vol.9, No.1, 556-566.

[13] Spalart, P.R., Deck, S., Shur, M.L., Squires, K.D., Strelets, M.K., and Travin, A., (2006). A new version of detached-eddy simulation, resistant to ambiguous grid densities. Theoretical Computational Fluid Dynamics, 20: 181-195.

[14] Shur K.L., Spalart P.R., Strelets M.K., and Travin A.K., (2008). A hybrid RANS-LES approach with delayed-DES and wall-modelled LES capabilities. International Journal of Heat and Fluid Flow, 29: 1638-1649.

[15] Keating A., and Piomelli U., (2006). A dynamic stochastic forcing method as a wall-layer model for large-eddy simulation. Journal of Turbulence, 7(12): 1-24.

[16] Deck S.,(2005a). Numerical simulation of transonic buffet over a supercritical airfoil. AIAA Journal, 43(7): 1556-1566.

[17] Deck S., (2005b). Zonal-detached eddy simulation of the flow around a high-lift configuration. AIAA Journal, 43(11): 2372-2384.

[18] Zhang, J.X., Sukhodolov, A.N., and Liu, H.(2014). Fully hydrodynamic versus hydrostatic modeling for shallow environmental flows, J.of Hydrodynamics, 26(4): 840-847.